Smart Structures and Systems, *Vol. 17, No. 1 (2016) 59-72*
DOI: http://dx.doi.org/10.12989/sss.2016.17.1.059

Enhanced impact echo frequency peak by time domain summation of signals with different source receiver spacing

Nils Ryden*

Engineering Geology, Faculty of Engineering, Lund University, Box 118, 22100 Lund, Sweden

(Received February 9, 2014, Revised June 2, 2015, Accepted August 7, 2015)

Abstract. The Impact Echo method can be used to measure the thickness of concrete plate like structures. Measurements are based on the identification of a clear thickness resonance frequency which can be difficult in very thick or highly attenuative plates. In this study the detectability of the measured resonant frequency is enhanced by time domain summation of signals with different source receiver spacing. The proposed method is based on the spatial and temporal properties of the first higher symmetric zero group velocity Lamb mode (S1-ZGV) which are described in detail. No application dependent tuning or filtering is needed which makes the method robust and suitable for implementation in automatic IE thickness measurements. The proposed technique is exemplified with numerical data and field data from a thick concrete wall and a highly attenuative asphalt concrete layer.

Keywords: impact echo; concrete; lamb wave; multichannel analysis of surface waves; MASW

1. Introduction

The Impact Echo (IE) method can be used to measure the thickness of a concrete plate like structure using low frequency stress waves. Developed in the 1980's at Cornell University (Sansalone and Carino 1986), the method has become a popular non-destructive test for concrete structures (Sansalone and Streett 1997, Popovics *et al*. 2006). In the conventional IE method the through thickness resonance frequency (f_r) is measured using an impact source and one receiver close to the source.

Traditionally, the method has been described and used as a local point test. More recently the IE method has been theoretically explained based on the zero group velocity point of the first higher symmetric Lamb wave mode (S1-ZGV) (Gibson and Popovics 2005). This theory has been able to explain and quantify the previously empirical correction factor β_{IE}=0.96 in the traditional empirical IE equation

$$f_r = \frac{\beta_{IE} V_P}{2h} \tag{1}$$

where V_P is the compression wave velocity and h is the thickness of the plate. But the Lamb wave

*Corresponding author, Associate Professor, E-mail: nils.ryden@tg.lth.se

http://www.techno-press.org/?journal=sss&subpage=8 ISSN: 1738-1584 (Print), 1738-1991 (Online)

theory can possibly provide further insights and improvements on the IE method. One implication from the theory is that the IE test is not as local as previously assumed. The IE resonance actually depends on the plate properties within a radius of several plate thickness from the source (Prada *et al*. 2008). This new insight opens up new possibilities for further improvements in the measurement set-up and data analysis.

A classical problem and source of error in IE testing is the presence of many additional peaks in the measured IE spectrum originating from reflections of both surface and body waves in a real 3D environment (Schubert *et al*. 2004). Time domain attenuation of large amplitude surface waves (Sansalone and Streett 1997), time frequency analysis (Abraham *et al*. 2000), and other data processing techniques such as the Hilbert–Huang transform (Algernon and Wiggenhauser 2007) and wavelet transform (Yeh and Liu 2008) have been proposed to increase the detectability and accuracy of the IE resonance peak. Recently, data processing methods based on two or more signals recorded at different distances from the source have also been proposed (Ryden and Park 2006a, Medina and Garrido 2007, Shokouhi 2009, Medina and Bayon 2010). Although not investigated in detail, these techniques benefit from the global mode shape of the S1-ZGV frequency.

In this study the identification of the measured IE resonance frequency is enhanced by simply summing time synchronized signals (from multiple impacts) within the global mode shape of the S1-ZGV mode. The proposed method is first theoretically explained based on Lamb wave theory and then demonstrated using both synthetic and field data. The proposed method is robust and therefore suitable for automatic processing in scanning IE measurements and/or in applications where the traditional IE method is difficult to use.

2. Theoretical analysis of zero group velocity Lamb waves

The proposed method, to enhance the IE peak, is based on theoretical properties of Lamb modes which are further described and analyzed in this section.

2.1 Lamb wave dispersion curves and excitability

Lamb waves (Lamb 1917) propagating in the plane of a free plate are only possible for certain combinations of f and in-plane wave number (k) corresponding to standing waves in the thickness direction. Possible combinations are given by the dispersion relation

$$\frac{tan(\beta h/2)}{tan(\alpha h/2)} = \left[\frac{-4\alpha\beta k^2}{(k^2-\beta^2)^2}\right]^{\pm 1} \tag{2}$$

where

$$\alpha^2 = \frac{\omega^2}{V_P^2} - k^2 \tag{3}$$

$$\beta^2 = \frac{\omega^2}{V_S^2} - k^2 \tag{4}$$

The ± sign on the right term of Eq. (1) represents, symmetric (+), and anti-symmetric (-), type

of wave propagation with respect to the mid plane of the plate (Graff 1975). Material stiffness properties are given by V_P and the shear wave velocity (V_S). Using the angular frequency ($\omega=2\pi f$), and the wave number ($k=\omega/c$), a root searching technique has to be used to calculate phase velocities (c) as a function of f, i.e. dispersion curves. An example of dispersion curves from the first three symmetric (S) and anti-symmetric (A) modes calculated from a reference plate model with Young's modulus (E) equal to 40 GPa, Poisson's ratio (ν) equal to 0.20, and h=0.15 m are plotted in Fig. 1. Phase velocities are plotted in Fig. 1(a) and group velocities (C_g) ($C_g=d\omega/dk$) in Fig. 1(b).

Points of zero group velocity (ZGV) in Fig. 1(b) correspond to strong thickness resonance modes of the plate (Tolstoy and Usdin 1957, Holland and Chimenti 2003, Prada *et al*. 2005). The IE thickness resonance mode is equal to the minimum frequency of the S1 mode at zero group velocity (S1-ZGV) (Gibson and Popovics 2005). For the reference case shown in Fig. 1 S1-ZGV is equal to 13 671 Hz, and marked with a black circle. At the S1-ZGV frequency the phase velocity is finite (here 7 023.6 m/s) (Meitzler 1965, Prada *et al*. 2008, Bjurström 2013). It can be noted that the A2 mode shows a similar behavior at 25 678 Hz marked with a gray circle and labeled A2-ZGV in Fig. 1.

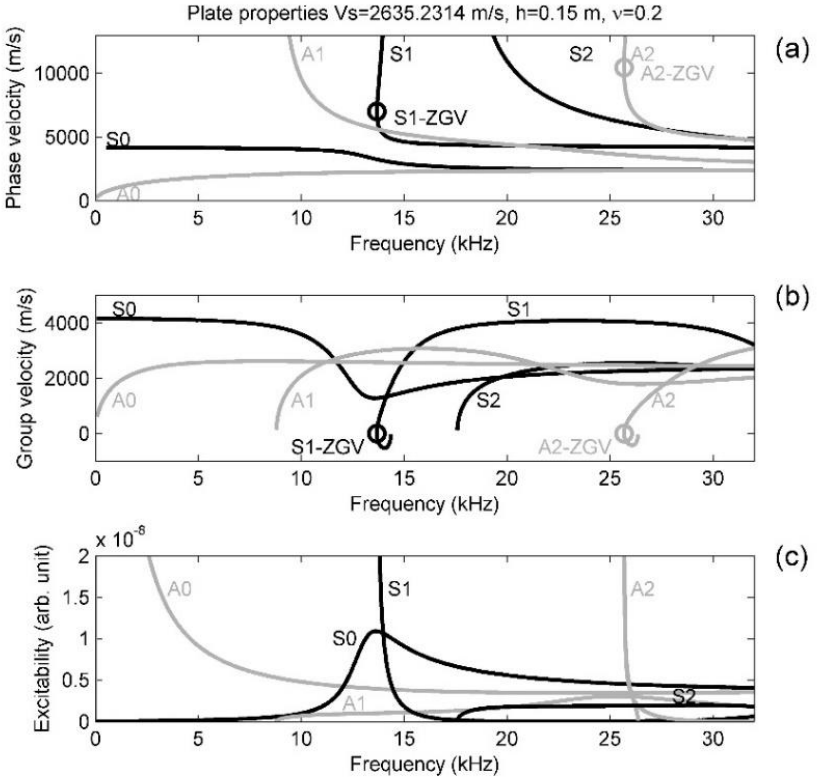

Fig. 1 Lamb wave dispersion curves for a free plate with E=40 GPa, ν=0.20, h=0.15 m (V_S=2635.2314 m/s). Thickness resonance frequencies S1-ZGV and A2-ZGV are marked with circles.

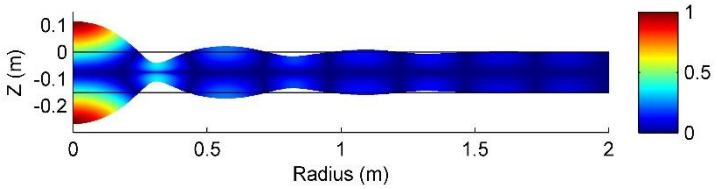

Fig. 2 Normal displacement field (absolute z-displacement) at the S1-ZGV frequency computed from a normal unit amplitude surface force at the center of the circular plate (within r<0.10 m)

The theoretical point excitability of a particular mode at a particular frequency is defined as the ratio of displacement of that mode to the applied force when both quantities are taken at the same location and direction (Wilcox 2004). Fig. 1(c) shows the predicted excitability of each Lamb mode from Figs. 1(a) and 1(b) calculated using the Disperse software (Disperse 2001). The excitability indicates the extent to which each mode is excited when the surface force is applied. The S1 mode clearly dominates the excitability at the S1-ZGV frequency, Fig. 1(c). It should also be noted that other modes (A0, S0, and A2) dominate other parts of the frequency range and can be utilized in a combined surface wave and IE analysis (Ryden and Park 2006a).

2.2 Spatial properties of the S1-ZGV mode

To study the spatial properties of the S1-ZGV mode, the frequency domain response at the S1-ZGV frequency is calculated from an axially symmetric 2D finite element model (Comsol 2013), using the same reference model (Fig. 2). The modeled plate is excited with a harmonic point force (r<0.10 m) in the normal direction along the surface of the plate. The relatively wide radius of the point source is used to enhance the S1-ZGV mode shape in Fig. 2. A convergence study on the predicted S1-ZGV frequency resulted in an axially symmetric free plate with a radius of 12.0 m, modeled using 124 000 tetrahedral second order elements with a maximum element size of 0.006 m. A 4 m long absorbing region is used to simulate infinite boundary conditions in the lateral direction (Castaigns *et al*. 2004). Using these settings the IE frequency could be predicted within 0.1% error range of the theoretical S1-ZGV frequency over a wide range of different ν. Material damping was introduced as a small loss factor (η) of 0.05% to broaden the predicted IE peak and make the response more realistic. η is the ratio between the imaginary part (loss modulus) and real part (storage modulus) of the complex E-modulus. It is interesting to observe that although most of the energy is confined close to the source normal displacements extend several plate thicknesses in the radial (r) direction.

2.3 The effect of Poisson's ratio on the S1-ZGV frequency and wavelength

The S1-ZGV mode is defined by both f and λ ($\lambda=c/f$) which are both dependent on ν. Fig. 3(a) shows a close up of the S1 Lamb wave dispersion curves around the S1-ZGV resonant mode at different values of ν. The exact positions of the S1-ZGV points are marked with circles in Fig. 3(a). At the S1-ZGV point both f and c increases slightly with increasing ν up to about ν=0.35 where c starts to increase more rapidly and approach infinity after ν=0.451 (Clorennec *et al*. 2007).

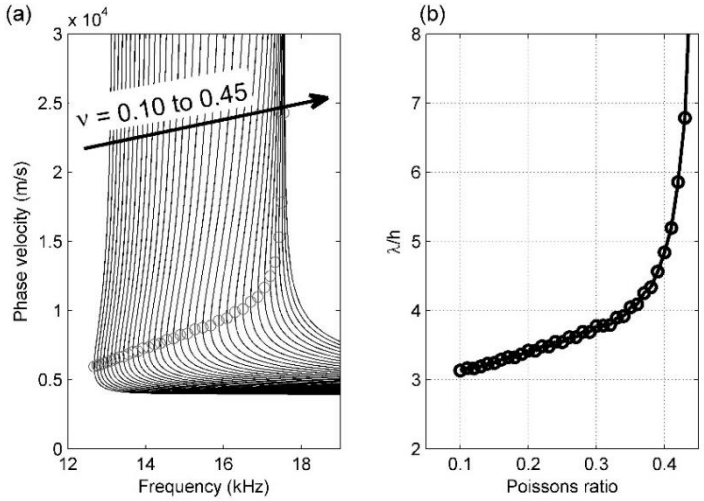

Fig. 3 (a) S1 dispersion curves as a function of ν with S1-ZGV frequencies and phase velocities marked with circles and (b) Corresponding wavelength (λ) to thickness (h) ratio as a function of ν at the S1-ZGV frequency

Fig. 3(b) shows the λ/h ratio as a function of ν for the S1-ZGV resonance mode calculated from the circles in Fig. 3(a). At Poisson's ratios lower than 0.35 (as for most asphalt concrete and concrete materials) the wavelength of the S1-ZGV mode ($\lambda_{S1\text{-}ZGV}$) is 3 to 4 times longer than the plate thickness. This means that within a radius of about *1.5h* from the source the plate surface is vibrating in phase at the S1-ZGV frequency (Fig. 2).

The above theoretical analysis of the properties of the S1-ZGV mode can be summarized using Fig. 1 through 3. At the S1-ZGV frequency the S1-ZGV mode has a finite wavelength and is dominating the response from a point source (Fig. 1). The S1-ZGV wavelength depends on ν and is about 3-4 times longer than the plate thickness in concrete (ν*~0.20*). The highest amplitudes are confined within the first nodal point which corresponds to about *1.5h* in concrete. (Figs. 2 and 3).

3. Time domain summation (TDS) technique

At each frequency the amplitude of a generated guided wave mode can be increased if the surface force function is in phase with the modal displacement along the surface (Viktorov 1967). From the theoretical analysis it can be concluded that the radial influence of the S1-ZGV mode extends several plate thicknesses in the radial direction from the source. The spatial extent of the S1-ZGV mode implies that the conventional IE point source could be wider in many typical applications. A source diameter close to $\lambda_{S1\text{-}ZGV}/2$ should be relatively much more efficient for the excitation of the S1-ZGV frequency (Balogun *et al.* 2007). A larger source diameter can be obtained synthetically by simply summing signals from multiple impacts at different distances from the receiver (source array), similar to phased array processing in ultrasonics or the vertical stack from a group of geophones in seismic reflection surveys. In addition the unknown velocities

of the plate can also be obtained from the same type of array measurements using the Multichannel Analysis of Surface Waves (MASW) method (Park *et al*. 1999, Ryden *et al*. 2004). However, the following analysis will be focused on the enhancement of the measured IE resonance frequency peak by time domain summation (TDS) of signals with different source-receiver separation. The summed signal $y_n(t)$ from a summation of n signals $x_i(t)$ at different distances i can be written as

$$y_n(t) = \sum_{i=1}^{n} x_i(t) \tag{5}$$

The Fourier transform is then applied to $y_n(t)$ to estimate the amplitude spectrum $Y(f)$ which is used to calculate a normalized power spectrum $Y_{norm}(f)$ as

$$Y_{norm}(f) = \frac{Y(f)^2}{\max\left(Y(f)^2\right)} \tag{6}$$

The S1-ZGV (or IE) resonance peak is then identified from the main peak in $Y_{norm}(f)$ instead of $Y_i(f)$. It should be noted that this TDS technique takes the phase information as a function of radius into account in the time domain summation (Eq. (5)).

3.1 Synthetic data examples

Two synthetic data examples are used to demonstrate the proposed TDS technique. The FE model described earlier has also been solved in time domain using a transient impulse source (125 μs long) at r<0.02 m. A smaller source radius is used here in order to mimic a typical impact source compared to the source radius used in Fig. 2 (r<0.10 m). Fig. 4(a) shows a typical multichannel record where amplitudes in each signal have been normalized with respect to the peak value of each signal. The S1-ZGV resonance frequency is initially masked by propagating modes but become visible at later times (t>0.7 ms) as an almost stationary damped frequency. The corresponding phase velocity spectrum (Park *et al*. 1999) is displayed along with matching theoretical fundamental mode Lamb waves (A0 and S0) to illustrate the accuracy of the reference model (Fig. 4(b)). The A0 and S0 dispersion curves are sensitive to the elastic constants in the plate (here V_S and ν) but not very sensitive to the thickness. The IE resonant frequency (from the power spectrum of the first signal) is more sensitive to the thickness and is compared to the theoretical S1-ZGV frequency in Fig. 4(c). The thicker solid line in Fig. 4(c) corresponds to $Y_{norm}(f)$ from a time domain summation (along the radial direction) of all signals in Fig. 4(a) (Eq. (2)). Both spectra display a clear peak at the correct theoretical S1-ZGV frequency (within 0.4% error range) in this ideal noise free example.

By simply summing all signals in time domain (Fig. 4(a)) the S1-ZGV resonance is amplified and all propagating waves are suppressed since they are not in phase over the radial offset range. The amplification of the S1-ZGV resonance is most efficient up to the first nodal point of normal displacement (here r=0.20 m) in the S1-ZGV mode shape (Fig. 2). The distance from the source to the first nodal point of the S1-ZGV mode depends on the plate properties (see Fig. 3) and is thus unknown in practice. However, since the amplitude of the S1-ZGV mode decreases rapidly with distance from the source it is not critical to sum signals up to the exact distance of the first nodal point. If many signals covering multiple nodal points are summed the resulting amplification is

any how dominated by the high amplitudes before the first nodal point (Fig. 2). After the first nodal point displacements are relatively much lower with alternating positive and negative displacements after each nodal point (Fig. 2). These lower amplitudes are basically averaged out if the summation includes multiple S1-ZGV wavelengths. It should be pointed out that with this method the estimated plate properties in Fig. 4 corresponds to a mean value over the complete offset range (here 1.0 m).

The cumulative change in the $Y_{norm}(f)$ is plotted in Fig. 5(a) by including signals further and further away from the source. The highest amplitude resonance peak stabilizes quickly and remain almost constant over a large range of radial distances included in the summation (Eq. (5)). An additional lower amplitude peak at 14 100 Hz appears just before 0.5 m distance (also visible in Fig. 4(c)). This peak may originate from the S1 cut off frequency which is expected at 14 344 Hz. Fig. 5(b) shows the corresponding image using the multicross-spectral density (MCSD) method proposed by Medina and Garrido (2007). In this technique the absolute value of the amplitude spectrum from each signal ($X_i(f)$) at each distance i from the source are successively multiplied in frequency domain. The resulting multicross-spectral density ($S_n(f)$) is defined as

$$S_n(f) = \prod_{i=1}^{n} |X_i(f)| \tag{7}$$

If $X_i(f)$ is dominated by a peak at the S1-ZGV frequency this peak will be significantly amplified in the successive multiplications resulting in a very clear and narrow peak at the correct S1-ZGV frequency. In the presented synthetic data example the MCSD method also enhances the identification of the S1-ZGV frequency very well (within 0.4% error range in Fig. 5(b)).

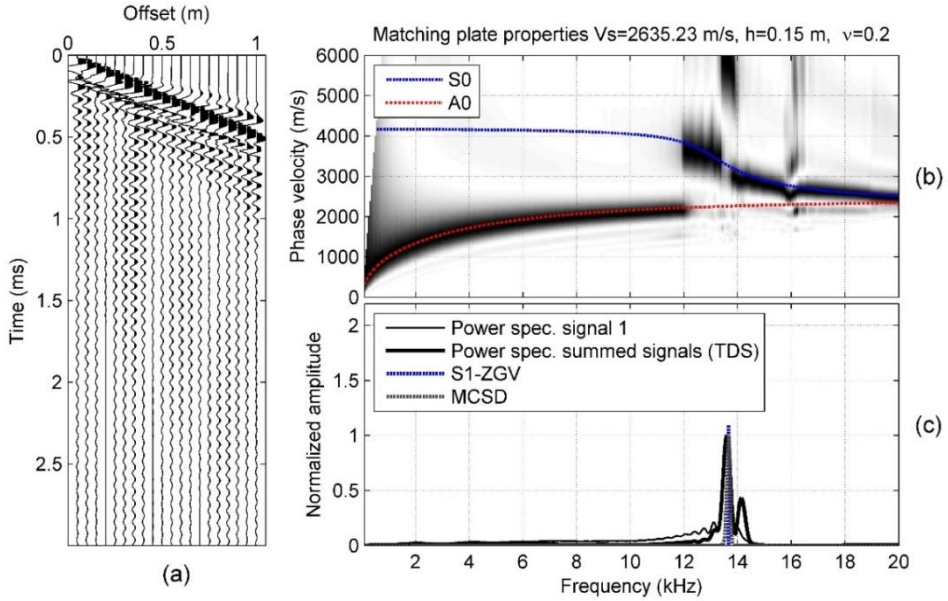

Fig. 4 (a) Synthetic data from the modelled reference plate, (b) Corresponding phase velocity spectrum with matching Lamb wave dispersion curves and (c) Amplitude spectrum from all summed signals in (a) with matching theoretical S1-ZGV resonant frequency

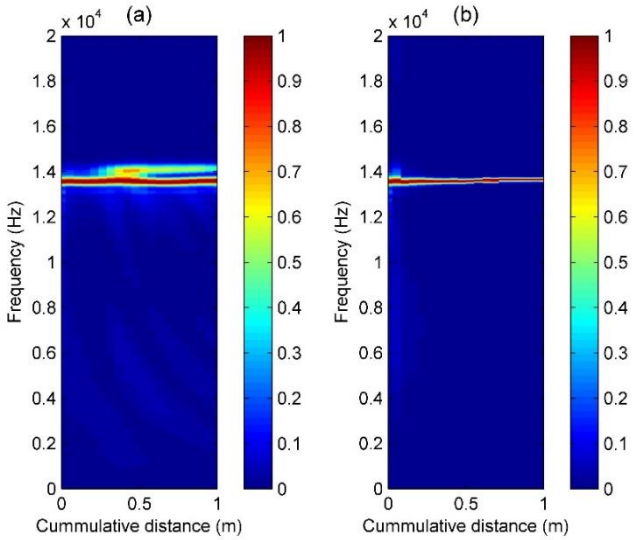

Fig. 5 Progression of the normalized power spectrum for data shown in Fig. 4 as a function of cumulative distance included in the process for (a) time domain summation (TDS) and (b) multicross-spectral density (MCSD)

However, it should be noted that the width of the spectral peak (i.e., attenuation) remain constant in the TDS technique while it becomes sharper and sharper in the MCSD method (Fig. 5(b)). A small upshift (0.7%) in peak frequency as a function of distance can be observed when zooming in on Fig. 5(b). This small upshift in S1-ZGV frequency with distance was also observed and pointed out by Prada *et al.* (2008). The same upshift is not visible in Fig. 5(a) where the peak instead oscillates with a frequency variation of 0.2% error range. Both of these variations in frequency with distance can be considered insignificant in most IE applications.

The main difference between the proposed TDS and the MCSD method is that the phase information is included and utilized in the TDS technique. Both methods benefit from the global 2D mode shape of the S1-ZGV frequency (Fig. 2). However, the cross spectral density method does not take advantage of the phase angle as a function of distance at the S1-ZGV frequency. By summing signals from different distances in time domain, propagating waves (out of phase) are suppressed and non-propagating resonances (in phase between nodal points of the S1-ZGV mode shape) are amplified. Medina and Garrido (2007) used a time domain window to suppress propagating surface waves before the MCSD is calculated. In the TDS technique propagating waves are automatically suppressed in the same process and no additional windowing and filtering procedures (which may depend on the actual thickness and surface wave velocity) are needed.

Although the MCSD method can be very efficient in many cases, the proposed TDS technique can be a better alternative in a real case scenario where the S1-ZGV resonance is not dominating the auto power spectrum at the closest distances from the source. To illustrate this point the axially symmetric model above is reduced in size to a radius of 1.3 m and the absorbing region is removed to generate reflected waves which interfere with the S1-ZGV resonance. The material loss factor is increased from 0.05% to a more realistic value for concrete at 2% at the S1-ZGV frequency

(corresponding to a beta factor of 2.27E-7 in Rayleigh damping $R_\beta = \eta/2\pi f$). A constant level of white noise is also added to each signal resulting in a signal to noise ratio from 49 dB to 39 dB in the first (r=0.05 m) and last (r=1.00 m) signal respectively. In this case the conventional IE signal is disturbed by random noise and body and surface wave reflections hindering a correct identification of the thickness resonance frequency (Schubert *et al*. 2004). The resulting synthetic data from the reduced model is plotted in Fig. 6. The reduced quality of the IE data is apparent in both time and frequency domain. However, in the power spectrum from the summed signals the correct S1-ZGV peak is still visible and enhanced compared to other disturbing lower frequency modes of the entire plate. In this case the peak from the TDS technique (13 566 Hz) is closer to the true value of the S1-ZGV frequency (13 671 Hz) compared to the conventional IE spectrum from the closest signal (13 401 Hz).

For comparison purposes the corresponding cumulative development of the TDS and MCSD method are plotted in Fig. 7. The highest amplitude peak from the TDS method (Fig. 7(a)) oscillates between 13401 Hz and 13621 Hz which is just below the expected S1-ZGV frequency (13671 Hz) and within 2% error range over the entire offset range. However, the highest amplitude peak from the MCSD method (Fig. 7(b)) jumps between different lower frequencies (5000-9000 Hz) and misses the expected S1-ZGV frequency at all distances except at the very first signal. Since the phase is not taken into account lower frequency propagating waves are also amplified in the MCSD method. These disturbances can be suppressed by using a time window and or additional frequency filtering (Medina and Garrido 2007), but these additional signal processing steps have to be fine-tuned for each application reducing the overall robustness. In the proposed TDS method propagating waves are automatically suppressed and resonance frequencies are amplified without any additional and application dependent filter in time or frequency domain.

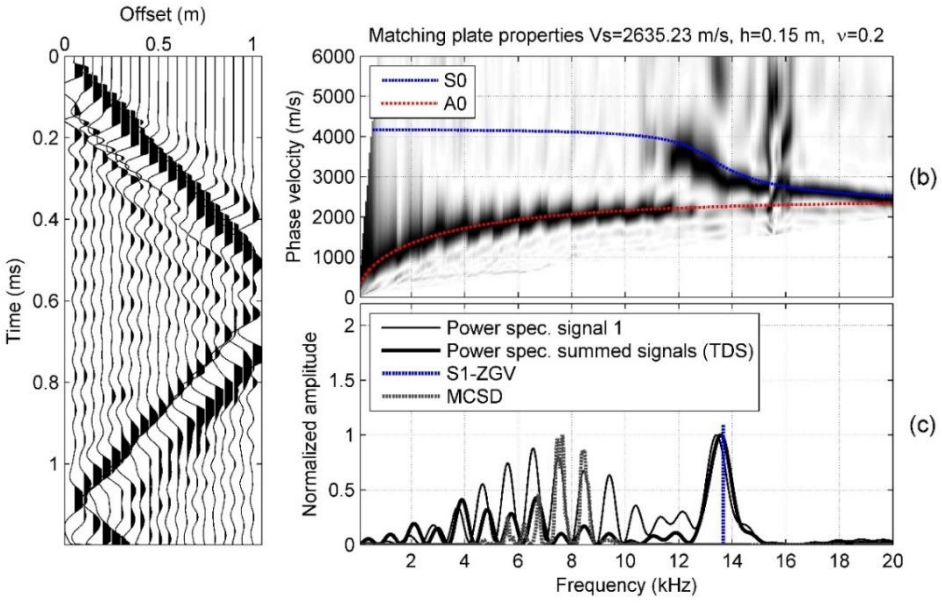

Fig. 6 (a) Synthetic data from the reference plate with reduced radius (r=1.3 m) and no absorbing region. (b) Corresponding phase velocity spectrum with matching Lamb wave dispersion curves. (c) Amplitude spectrum from all summed signals in (a) with matching theoretical S1-ZGV resonant frequency

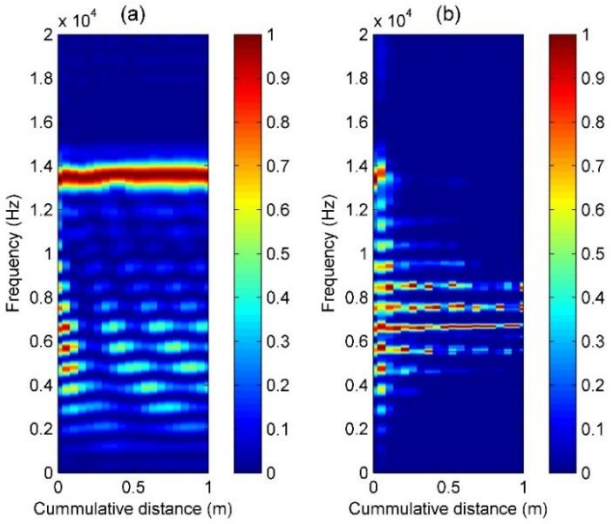

Fig. 7 (a) Progression of the normalized power spectrum for data shown in Fig. 6 as a function of cumulative distance included in the process for (a) time domain summation (TDS) and (b) multicross-spectral density (MCSD).

3.2 Field test examples

To further demonstrate the enhancement of the IE frequency peak by the TDS method two different field test examples are presented below. In the first example MASW data was collected along a 1.0 m thick concrete wall using one fixed accelerometer at r=0.00 m and multiple impacts from 0.05 m to 2.65 m with 0.05 m between impact points as proposed in Ryden *et al.* (2004). The assembled multichannel record is presented in Fig. 8(a) along with the spectra from the TDS and MCSD methods in Fig. 8(c). The expected IE resonance frequency should appear close to 2000 Hz since the V_P was estimated to about 4300 m/s (Eq. (1)). The power spectrum from the TDS method shows a clear peak at 1890 Hz. In this case the frequency range of the impact source is relatively high compared to the IE resonance frequency, which can be seen in the spectrum from the first signal (dx=0.05 m) in Fig. 8(c). In this type of situation the MCSD technique can amplify a different higher frequency peak in the data which can be seen in Fig. 8(c). The exact cause of the higher frequency peaks in Fig. 8(c) is not known but they could possibly correspond to higher resonance modes in the thickness direction of the concrete wall.

The automatic suppression of propagating waves and amplification of resonance frequencies is further illustrated in Fig. 9 where all raw data signals are plotted along with the summed signal. The summed signal reveals a decaying almost monochromatic signal with a period of about 0.5 ms corresponding to the peak frequency (1890 Hz) in the power spectrum from the summed signal (Fig. 8(c)). It should be noted that the first part of the signal with high amplitude surface waves are only amplified with a factor 2 although 53 signals have been summed. The IE resonance is amplified with a factor of about 15 at t~0.010 s. This relative suppression of propagating waves and amplification of the IE frequency is obtained automatically in the summed signal without any additional windowing and filtering procedures.

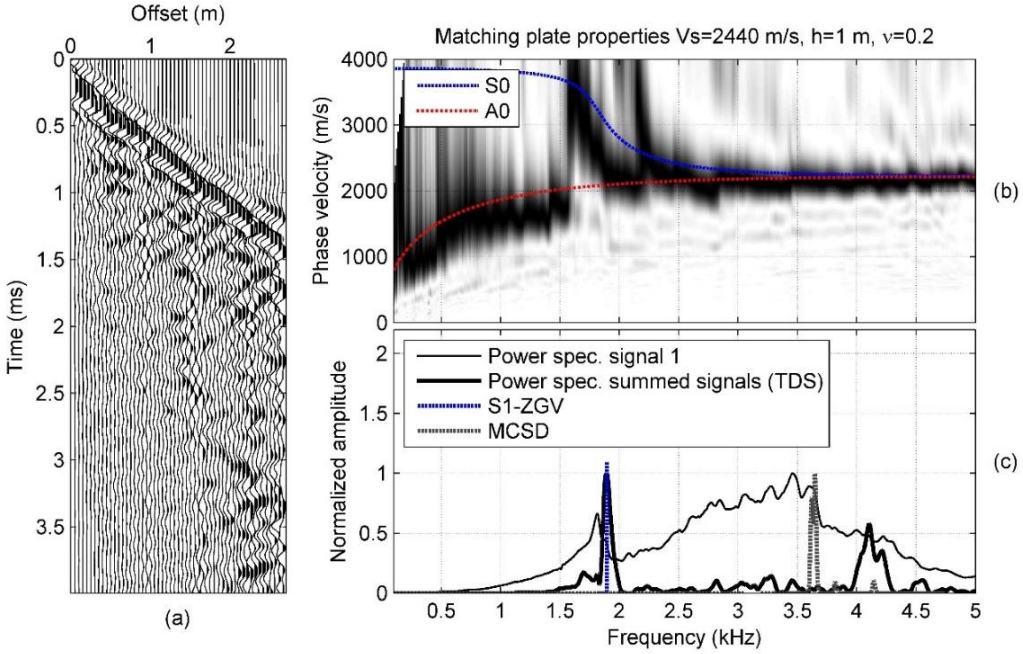

Fig. 8 (a) Recorded data along a 1.0 m thick concrete wall, (b) Corresponding phase velocity spectrum with matching Lamb wave dispersion curves and (c) Amplitude spectrum from all summed signals in (a) with matching theoretical S1-ZGV resonant frequency

In the second example, MASW data were collected over a flexible pavement with a 0.13 m thick asphalt concrete layer (13 deg C), Fig. 10. Asphalt concrete pavements are usually difficult to test with the IE method because measured signals are heavily attenuated. Matching plate properties (V_S=2145 m/s, h=0.133 m, and ν=0.25) compares well with the true thickness (0.13 m) and reasonable high frequency asphalt concrete properties (Ryden and Park 2006b), Fig. 10. The resonant frequency peak from the summed signals (Fig. 10(c)) is clearly detectable, and in this case it is the key property to estimate a correct thickness of the top asphalt concrete layer. The power spectrum from the first signal has a smaller peak at a slightly higher frequency (14.7 kHz). This vague peak demonstrates that the conventional IE method can be difficult to apply on asphalt concrete layers. All spectra in Fig. 10(c) also displays a few lower frequency peaks which may originate from the complete multilayer pavement system.

It should also be noted that the resonance peak from the summed signals (thick solid TDS curve in Fig. 10(c)) seems to capture the relatively large material attenuation in asphalt concrete. The quality factor (Q) is the inverse of η and can be calculated in frequency domain as the ratio between f_r and the width (Δf) of the resonant peak at half-power of the peak amplitude (half-power bandwidth method $Q=fr/\Delta f$). In this case Q can be estimated as ~6 from the TDS curve in Fig. 10(c), which is a reasonable value for asphalt concrete at this frequency and temperature (Gudmarsson *et al*. 2012).

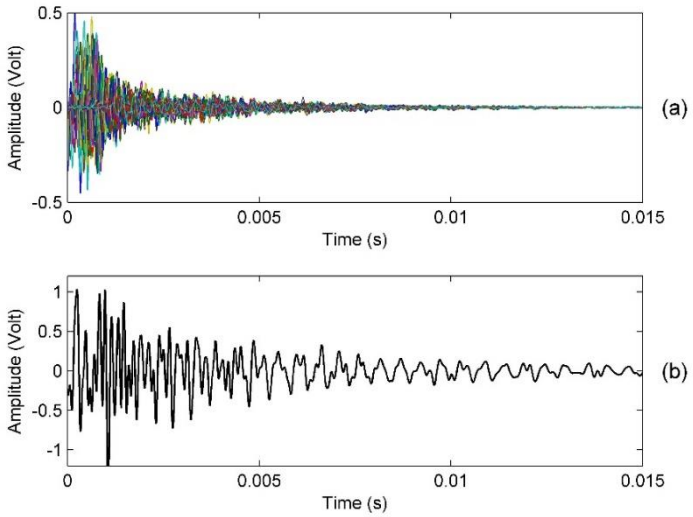

Fig. 9 (a) All 53 recorded signals from the concrete wall example and (b) Summed signals (TDS method) revealing the IE resonance frequency

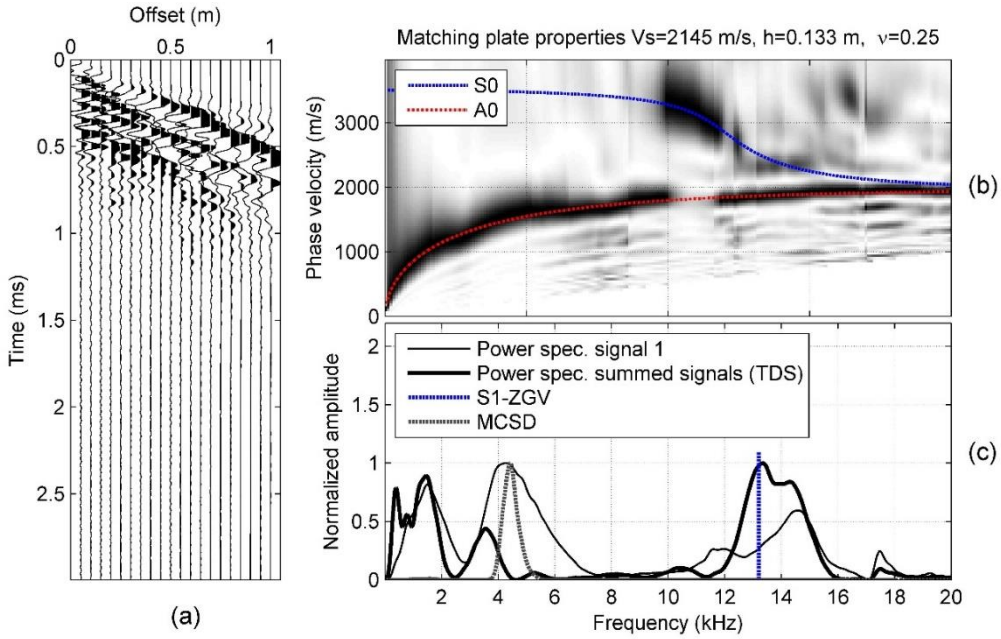

Fig. 10 (a) Recorded data over an asphalt pavement, (b) Corresponding phase velocity spectrum with matching Lamb wave dispersion curves and (c) Amplitude spectrum from all summed signals in (a) with matching theoretical S1-ZGV resonant frequency.

5. Conclusions

A simple multichannel processing technique based on time domain summation (TDS) of signals with different source receiver spacing have been presented in this study.

- The proposed method can enhance the identification of the Impact Echo (IE) peak in situations where conventional IE measurements are difficult.
- Propagating waves are automatically suppressed and resonance frequencies are amplified without any additional windowing and filtering procedures. The method is therefore suitable for automatic IE data processing.
- The proposed method is based on the spatial and temporal properties of the S1-ZGV Lamb mode which are theoretically described in detail.

Acknowledgments

The research described in this paper was financially supported by the Swedish Research Council for Environment, Agricultural Sciences and Spatial Planning (Formas), the Swedish Transport Administration (TRV), and the Swedish construction industry's organization for research and development (SBUF)

References

Abraham, O., Lonard, C., Cte, P. and Piwakowski, B. (2000), "Time frequency analysis of impact-echo signals: numerical modeling and experimental validation", *ACI Mater. J.*, **97**(6), 645-657.

Algernon, D. and Wiggenhauser, H. (2007), "Impact echo data analysis based on Hilbert–Huang transform", *Transport. Res. Rec.*, **2028**, 146-153.

Balogun, O., Murray, T.W. and Prada, C. (2007), "Simulation and measurement of the optical excitation of the S1 zero group velocity Lamb wave resonance in plates", *J. Appl. Phys.*, **102**, 064914.

Bjurström, H. and Ryden, N. (2013), "Air-coupled detection of the S1-ZGV lamb mode in a concrete plate based on backward wave propagation", *Proceedings of the 39th annual review of progress in quantitative nondestructive evaluation, AIP Conf. Proc.*, **1511**, 1294.

Castaings, M., Bacon, C., Hosten, B. and Predoi, M.V. (2004), "Finite element predictions for the dynamic response of thermo-viscoelastic material structures", *J. Acoust. Soc. Am.*, **115**, 1125-1133.

Clorennec, D., Prada, C. and Royer, D. (2007), "Local and noncontact measurement of bulk acoustic wave velocities in thin isotropic plates and shells using zero-group velocity Lamb modes", *J. Appl. Phys*., **101**, 034908.

Comsol (2013), *User's Guide*, Version 4.3 by COMSOL AB 2013, http://www.comsol.com.

Disperse (2001), *A system for generating dispersion curves*, User's manual version 2.0.11. Software version 2.0.15e. Guided Ultrasonics, London.

Gibson, A. and Popovics, J. (2005), "Lamb wave basis for impact-echo method analysis", *J. Eng. Mech. - ASCE*, **131**(4), 438-443.

Graff, K.F. (1975), *Wave propagation in elastic solids*, Dover Publications, New York, ISBN 0-486-66745-6.

Gudmarsson, A., Ryden, N. and Birgisson, B. (2012), "Characterizing the low strain complex modulus of asphalt concrete specimens through optimization of frequency response functions", *J. Acoust. Soc. Am.*, **132**(4), 2304-2312.

Holland, S.D. and Chimenti, D.E. (2003), "Air-coupled acoustic imaging with zero-group-velocity lamb

modes", *Appl. Phys. Lett.*, **83**(13), 2704-2706.
Lamb, H. (1917), "On waves in an elastic plate", *Proc. Roy. Soc. A.*, **93**, 114-130.
Medina, R. and Garrido, M. (2007), "Improving impact-echo method by using cross-spectral density", *J. Sound Vib.*, **304**, 769-778.
Medina, R. and Bayón, A. (2010), "Elastic constants of a plate from impact-echo resonance and Rayleigh wave velocity", *J. Sound Vib.*, **329**, 2114-2126.
Meitzler, A.H. (1965), "Backward-wave transmission of stress pulses in elastic cylinders and plates", *J. Acoust. Soc. Am.*, **38**, 835-842.
Park, C.B., Miller, R.D. and Xia, J. (1999), "Multichannel analysis of surface waves", *Geophysics*, **64**(3), 800-808.
Popovics, J.S., Cetrangolo G.P. and Jackson N.D. (2006), "Experimental investigation of impact-echo method for concrete slab thickness", *J. Korean Soc. Nondestruct. Test.*, **26**, 427-439.
Prada, C., Balogun, O. and Murray, T.W. (2005), "Laser based ultrasonic generation and detection of zero-group velocity Lamb waves in thin plates", *Appl. Phys. Lett.*, **87**, 194109.
Prada, C., Clorennec, D. and Royer, D. (2008), "Local vibration of an elastic plate and zero-group velocity Lamb modes", *J. Acoust. Soc. Am.*, **124**(1), 203-212.
Ryden, N., Park, C.B., Ulriksen, P. and Miller, R.D. (2004), "Multimodal approach to seismic pavement testing", *J. Geotech. Geoenviron. Eng. - ASCE*, **130**(6), 636-645.
Ryden, N. and Park, C.B. (2006a), "A combined multichannel impact echo and surface wave analysis scheme for non-destructive thickness and stiffness evaluation of concrete slabs", *Proceedings of the 6th Int. Symp. on NDT in Civil Engineering*, Saint Louis, Missouri, United States, August.
Ryden, N., and Park, C.B. (2006b), "Fast Simulated Annealing Inversion of Surface Waves on Pavements using Phase Velocity Spectra", *Geophysics*, **71**(4), 49-58.
Sansalone, M. and Carino, N.J. (1986), Impact-echo: A method for flaw detection in concrete using transient stress waves, *Rep. No. NBSIR 86-3452, National Bureau of Standards*, Gaithersburg, Md.
Sansalone, M.J. and Streett, W.B. (1997), *Impact-echo: Non-destructive evaluation of concrete and masonry*, Bullbrier, Ithaca, N.Y.
Schubert, F., Wiggenhauser, H. and Lausch, R. (2004), "On the accuracy of thickness measurements in impact-echo testing of finite concrete specimens—numerical and experimental results", *Ultrasonics*, **42**, 897-901.
Shokouhi, P. (2009), "Two-channel Impact Echo", *Proceedings of the 7th Int. Symp. on Non-Destructive Testing in Civil Engineering (NDTCE'09)*, Nantes, France, June.
Tolstoy, I. and Usdin, E. (1957), "Wave propagation in elastic plates: Low and high mode dispersion", *J. Acoust. Soc. Am.*, **29**(1), 37-42.
Yeh, P.L. and Liu, P.L. (2008), "Application of the wavelet transform and the enhanced Fourier spectrum in the impact echo test", *NDT&E Int.*, **41**, 382-394.
Viktorov, I.A. (1967), *Rayleigh and Lamb Waves*, New York: Plenum Press.
Wilcox, P. (2004), "Modeling the excitation of Lamb and SH waves by point and line sources", *Review of Progress in Quantitative NDE*, (Eds., D.O. Thompson and D.E. Chimenti), *American Institute of Physics*, New York, **23**, 206-213.